Received: 28 June 2022 | Revised: 24 July 2022 | Accepted: 24 July 2022

DOI: 10.1002/agt2.260

Aggregate WILEY

RESEARCH ARTICLE

A family of oligo(p-phenylenevinylene) derivative aggregation-induced emission probes: Ultrasensitive, rapid, and anti-interfering fluorescent sensing of perchlorate via precise alkyl chain length modulation

Fangfang Xiao[1,2] | **Yushu Li**[1] | **Jiguang Li**[1,2] | **Da Lei**[1] | **Guangfa Wang**[1] | **Tianshi Zhang**[1,2] | **Xiaoyun Hu**[1,2] | **Xincun Dou**[1,2]

[1]Xinjiang Key Laboratory of Explosives Safety Science, Xinjiang Technical Institute of Physics & Chemistry, Chinese Academy of Sciences, Urumqi, China

[2]Center of Materials Science and Optoelectronics Engineering, University of Chinese Academy of Sciences, Beijing, China

Correspondence
Xincun Dou, Xinjiang Key Laboratory of Explosives Safety Science, Xinjiang Technical Institute of Physics & Chemistry, Chinese Academy of Sciences, Urumqi 830011, China.
Email: xcdou@ms.xjb.ac.cn

Fangfang Xiao and Yushu Li contributed equally to this work.

Funding information
Natural Science Foundation of Xinjiang, Grant/Award Number: 2022D01E03; West Light Foundation of the Chinese Academy of Sciences, Grant/Award Number: 2021-XBQNXZ-023; National Natural Science Foundation of China, Grant/Award Numbers: 52172168, 22104152; Key Research Program of Frontier Sciences, CAS, Grant/Award Number: ZDBS-LY-JSC029

Abstract

The precise regulation of interactions provided by aggregation-induced emission (AIE) probes is of considerable significance for improving the sensing performance in the field of on-site detection. Here, a highly sensitive perchlorate detection probe was designed by precisely modulating the van der Waals interactions by adjusting the length of the alkyl chain. The optimized AIE probe demonstrated superior perchlorate detection performance owing to its strong van der Waals interactions with perchlorate, including a low detection limit (53.81 nM), rapid response (<5 s), and excellent specificity even in the presence of 16 interfering anions. In addition, a hydrogel-based device loaded with the probe was constructed to achieve ultrasensitive recognition of perchlorate particles with a detection limit as low as 15 fg under a fluorescence microscope. Moreover, the practicality of the probe was further verified by employing a sensing chip in a portable detector, and thus the probe has been proven to be highly promising for trace perchlorate monitoring in real scenarios. We expect the present study to be of great value for the efficient design of high-performance fluorescent probes.

KEYWORDS
aggregation-induced emission, explosive detection, fluorescent probe, perchlorate, trace sensing

1 | INTRODUCTION

Accurate, sensitive, and rapid detection and identification of toxic and harmful anions is of great importance because they can effectively prevent human beings from environmental pollution and terrorist attack.[1] For detecting and identifying toxic and harmful anions, great efforts have been devoted to fluorometry,[2] colorimetry,[3] Raman spectroscopy,[4] ion migration spectrometry,[5] and electrical methods[6] to explore pioneering methods. Among them, benefiting from adjustable structure, diverse functional groups and high luminescence efficiency, organic fluorescent probes have been widely used in biological imaging,[7] ion analysis,[8] explosive detection,[9] gas sensing,[10] etc. Regarding the fluorescence behaviors, fluorophores for high-performance probes design can be divided into aggregation-induced quenching (ACQ) and aggregation-induced emission (AIE).[11] Among them, AIE fluorophores, such as tetraphenylethylene, hexaphenylsilole, oligo/polyphenylenevinylenes, and so on, owing to their unique optical characteristics of weak emission in dispersion but high emission efficiency in aggregation or the solid state, provide a solution to the concentration-induced quenching problem of traditional organic dyes and have been widely studied in the field of ion detection.[12] The basic origin for utilizing the AIE characteristic phenomenon is to restrict intra/inter molecular motion and hence control the non-radiative decay pathways.[13] In the AIE principle-based detection

field, for reactive electron-rich anions, such as CN^-, F^-, and HSO_3^-, it is feasible to design probes by introducing electron-deficient groups, such as C=C bond and C=N bond, allowing nucleophilic addition reaction. The sensing could be achieved with high sensitivity and specificity by fluorescence quenching due to the reaction, blocking the photoinduced electron transfer (PET) process, or fluorescence enhancement due to excited-state intramolecular proton-transfer (ESIPT) process recovery.[14] However, for non-coordination and non-reactive anions with dispersed charges, such as NO_3^- and ClO_4^-, only weak interactions, such as hydrogen bonds, electrostatic force, and anion–π interactions could be utilized to design AIE probes, which generally lead to low sensitivity and specificity.[15] To improve the sensitivity and specificity of the AIE probe, the microenvironmental hydrophilicity and hydrophobicity can be regulated to affect the non-covalent weak interactions between the AIE probe and anions,[16] and then influence the aggregation size and number of the AIE probe, resulting in the variation in the detection performance. From the perspective of modulating the chemical structure of probes, including changing the core of AIE and the auxiliary group[17] of the dipyridinium salt, or changing the number of recognition sites of wax salt and the length of the flexible chain, the structure of the AIE probe is crucially important for promoting the detection performance. However, the underlying mechanism of how the specific probe molecular structure can precisely modulate the resulting sensitivity and specificity is still unclear. It is of great significance for the directional design of a highly efficient functional probe.

Perchlorate, as a typical charge-dispersion-type non-coordination and non-reactive anion,[18] is a strong oxidizer, and could cause combustion and explosions when mixed with organic substances or reducing agents. It has been used as an important raw material for manufacturing improvised explosive devices,[19] which would cause a more severe threat to world security with readily available raw materials compared to tightly controlled military explosives. According to the 2018 explosive incident report of the United States Bomb Data Center, perchlorates are responsible for more than 60% of the worldwide explosion incidents in the past few years.[20] Moreover, because of its regular tetrahedral structure, resulting in non-volatility, high stability, and solubility, perchlorate can be a ubiquitous environmental contaminant,[21] occurring in a wide range of foods, including vegetables, fruit, milk, and dairy products.[22] Due to the risk of perchlorate accumulation in the human body inhibiting iodine utilization,[23] the European Commission (EU) issued Regulation 2020/685 amending maximum levels of perchlorate in certain foods as low as 0.01 μg/kg.[24] Therefore, the highly sensitive detection of perchlorate is of great significance to environmental protection, public health, and homeland security. Although some attempts have been made to detect perchlorate using organic probes,[25] most of them suffer from high sensitivity and specific selectivity owing to the charge-dispersion nature of perchlorate anion. Although a few of them achieved enhanced sensitivity and specificity by molecular structure regulation from the aspect of hydrophilic and hydrophobic consideration,[26] the underlying mechanism remains unclear. Furthermore, the presence of a non-negligible background signal restricts the practical application of the probe. To address these issues, exploring a new methodology for specifically and rapidly distinguishing perchlorate with minimal background interference is highly demanded but remains a challenge.

Herein, rapid and sharp turn-on fluorescence detection of perchlorate anions with high sensitivity and anti-interference capability was realized by effectively modulating the van der Waals forces between perchlorate and the as-designed oligo(p-phenylenevinylene) derivative AIE probe by varying the alkyl chain's length. The investigation of the role of the alkyl chain's length in the probe revealed that the most remarkable restriction of the single-probe motion could be achieved by the probe with the octyl chain (C8) in the presence of perchlorate owing to strong intermolecular interaction. Consequently, a detection limit as low as 53.81 nM perchlorate resulted in the emergence of green fluorescence emission (530 nm) within 5 s with good selectivity and excellent anti-interference capability. In addition, a hydrogel-based device incorporated with the C8 probe was constructed to achieve ultrasensitive recognition of perchlorate particles with a detection limit as low as 15 fg under a fluorescence microscope. Furthermore, the detector-based ultra-fast on-site identification of perchlorates in simulated circumstances, such as security checkpoints, entrance, and the trunk of the car, further verified the reliability of the present probe modulation strategy in advancing probe utilization in practical scenarios.

2 | RESULTS AND DISCUSSION

2.1 | Influence of precise modulation of alkyl chain on the sensitivity of the AIE probe to perchlorate

The core idea of the proposed probe design strategy is to precisely modulate the van der Waals interaction between the probe and perchlorate by tuning the alkyl chain length (with the C atom number from 3 to 9) of the oligo(p-phenylenevinylene) derivative AIE probe (C3–C9 probe) with cyano and phenyl substituents as optical property regulation sites and pyridinium as the recognition site (Figure 1A). Although these oligo(p-phenylenevinylene) derivatives have subtle structural modifications (Figures S1–S11), it can be proved that all C3–C9 probes are AIE molecules according to the AIE characteristic curves of C3–C9 in different proportions of good (DMSO) and poor (water) solvents (Figures S12–S18). With an increase in the alkyl chain length, the fluorescence emission of the dilute solution of the probes remained low and unchanged except for the C9 probe (Figure S19a). The much stronger fluorescence emission of C9 probe was generated due to the self-aggregation with the aggregation size of about 1 μm, which is 200 times larger than that of C3 and C8 (Figure S19b), demonstrating that the chain length is sufficient to modulate the hydrophobicity and hence the aggregation behavior of the probe. After adding 1 equiv of perchlorate, all C3–C9 probes with same concentration showed a fluorescence-on phenomenon due to probe aggregation induced by perchlorate, and the C8 probe showed the most prominent emission compared with the other probes in the fluorescent images under 365 nm UV light illumination (Figure 1B). From the extraction of the corresponding green values of the fluorescent images (Figure 1C), it can be

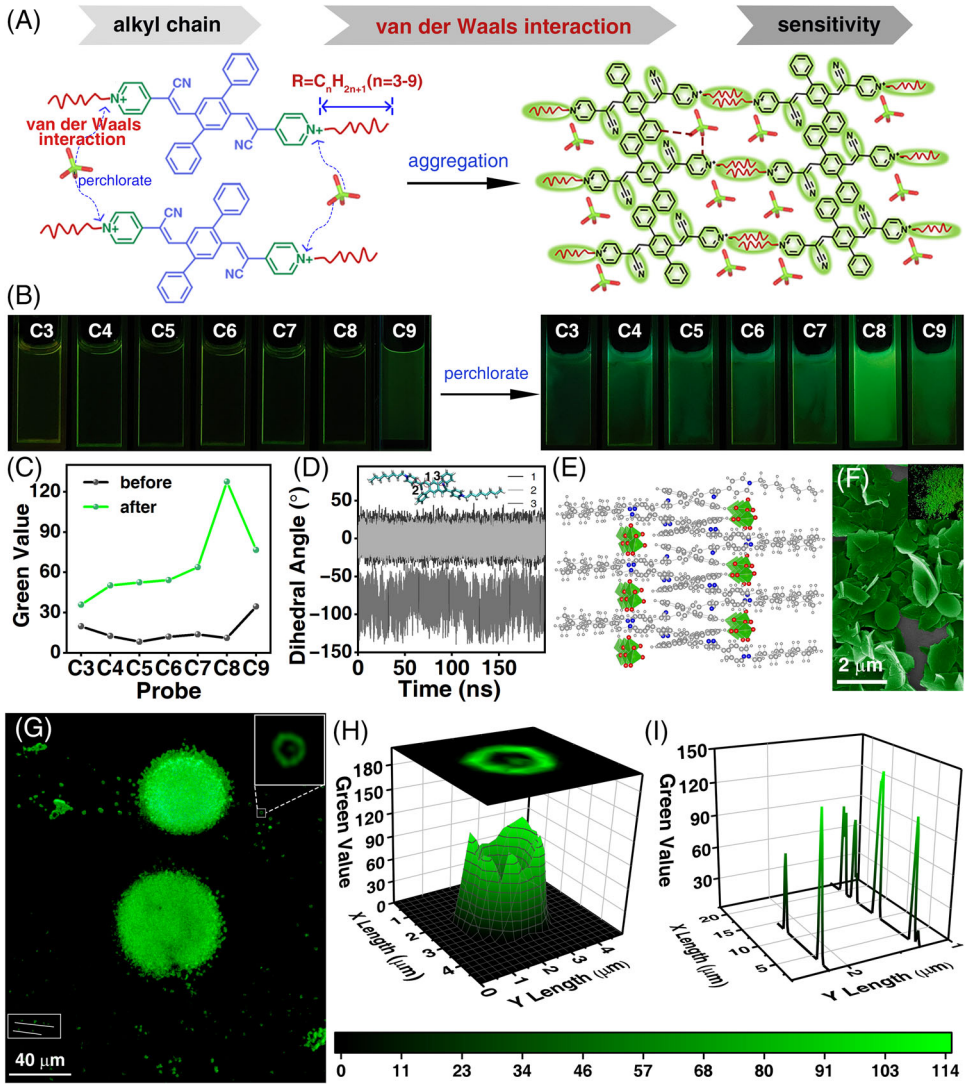

FIGURE 1 (A) Schematic illustration of the precise modulation of alkyl chains in the aggregation-induced emission probe for the regulation of its sensitivity toward perchlorate. (B) Fluorescent images of C3–C9 probes (2 mM) in the mixture solution of ethylene glycol/0.1 M citric acid (3:2, v/v) before and after perchlorate addition under 365 nm UV light and (C) the corresponding green values. (D) The dihedral angle between inner diphenyl-substituted phenylene and the vinylene units (1), the vinylene units and the outer pyridinium rings (2), as well as the phenyl substituents and the phenylene core (3) of the C8 probe. (E) The single-crystal structure and (F) scanning electron microscopy image of the aggregate product of the optimized probe (C8) and perchlorate with the fluorescent image of the aggregate powder as inset. (G) Dark-field fluorescence images of the C8 probe when analyzing various sizes of perchlorate microparticles. (H) 3D colormap surface analysis of the selected fluorescent area caused with diameter of 2.33 μm by a perchlorate particle. (I) Line scan of the selected area for rapid identification of perchlorate microparticles

found that the C8 probe is more sensitive than C3–C7 and C9 probes to perchlorate with the maximum fluorescence change and the quantum yield boosted by 60 times from 0.43% to 25.91% before and after detection. In general, the increase of the alkyl chain length leads to the enhancement of the probe detection efficiency toward perchlorate (Figure S20). However, a further increase in the C number from 8 to 9 in the alkyl chain would not help to enhance the detection efficiency due to the self-aggregation of the C9 probe, making the C8 probe the most efficient probe. Therefore, it can be concluded that modulating the length of the alkyl chain in the presented oligo(p-phenylenevinylene) derivative AIE probe is an effective strategy to achieve the best response for perchlorate detection. To further investigate the fluorescence-on mechanism of the AIE probes after the sensing process, the molecular dynamics simulation and the single-crystal structure analysis were performed. From the molecular dynamics simulation result of a single C8 probe molecule with H_2O as model solvent, the molecule was constantly in motion driven by C—C single bond rotation (Video S1). For instance, the dihedral angles in the C8 probe between the inner phenylene core and the vinylene units, the vinylene units and the outer pyridinium rings, as well as the phenyl substituents and the phenylene core spontaneously change rapidly in the range of −50° and 50°, −30° and 30°, −30° and −150°, respectively (Figure 1D). The continuous molecular motion leads to the energy dissipation in a non-radiative decay pathway, conducing to very weak or even no fluorescence emission. From the single-crystal structure analysis of the aggregation product from C8, it is obvious that the cationic probe molecules were assembled in a regular cross arrangement, in which one probe was bound with two perchlorates with the dihedral angles of the inner diphenyl-substituted phenylene and the vinylene units, the vinylene units and the outer pyridinium rings, and the phenyl functionalities and the phenylene center of the C8 probe fixed at 35.6°, 32.2°, and 145.2°, respectively (Figure 1E and Table S1). Therefore, the rigid restriction of intra/intermolecular

motion (RIM) of the probe molecule in the crystal leads to a strict control over non-radiative decay pathway to ensure that the radiative decay pathway is the only excitation energy dissipation path, resulting in the bright green fluorescent emission of the aggregates. Revealed by scanning electron microscopy (SEM), the green fluorescence emitting powder of the aggregation product has the flake-shaped morphology with diameter of several microns, which is more than 50 folds larger than that of the self-aggregation of C8 probe (Figure S21), further proving that the sharp emission of the powder was caused by perchlorate-induced aggregation (Figure 1F).

The fluorescence of this C8 probe could even be visualized directly by perchlorate microparticles in a wet environment. When the C8 probe was embedded in a polyacrylamide (PAM) hydrogel to capture airborne perchlorate particles, green fluorescence signal was clearly observed with diameters in the range of 2 to 60 microns (Figure 1G). Most importantly, the C8 probe dispersed in the PAM hydrogel showed no fluorescence, but green fluorescence appeared immediately in the region of perchlorate microparticles, indicating the excellent fluorescence performance. A representative particle with the diameter as small as nearly 2.33 μm (16.69 pg) could be clearly identified in the enlarged view. The 2D fluorescent pattern of a selected region was finely simulated by extracting the green value (Figure 1H). As a result, the 3D color map surface transformed from the 2D fluorescent pattern exhibited more detailed morphological information, which is helpful for understanding the remarkable change in fluorescence. Sharp intensity increase (Figure 1I) could be obtained by the line scan of selected region in Figure 1F, which corresponds to the location of the fluorescent dots, demonstrating that the C8 probe is promising for fluorescence-on detection of perchlorate microparticles owing to the large emission contrast.

2.2 | The role of alkyl chain length in determining the sensitivity difference to perchlorate and the detailed analysis of the aggregates

To discover the intrinsic reason for why C8 has the most sensitive response, molecular dynamics simulations of the C3–C9 probes with and without perchlorate were carried out. Within the simulation time scale of 200 ns, all the probes showed a scatter phenomenon with no apparent difference (Figure 2Ai). However, in the presence of perchlorate, different clustering conditions were observed. C4–C6 formed multiple clusters with different sizes, while C3 and C7 remains ununited. Meanwhile, C8 and C9 formed single clusters, and the cluster formed by C8 is more condensed than C9 (Figure 2Aii). Furthermore, the quantitative analysis of the radius of gyration results extracted from dynamic simulations in time interval of 100–200 ns, showed that C8 and C9 had the smallest radius of gyration, representing the lowest degree of system looseness and hence the largest aggregation size (Figure 2B). Considering the self-aggregation of C9 before detection, C8 is the most efficient probe for aggregating with perchlorate induction. It is suspected that the alkyl chain of the probe greatly impacts its interactions with perchlorate, thereby affecting the aggregation state of the probe. To thoroughly investigate the interactions between probe and perchlorate, the average non-covalent interaction (aNCI) was calculated from the molecular dynamics simulation trajectory by taking C8 as an example. The predominant interaction between C8 probe and perchlorate was van der Waals forces represented by the green region (Figure 2C). In addition, a statistical analysis showed that the van der Waals interaction energy between the C8 probe and perchlorate was the strongest among the C3–C9 probe family (Figure 2D), confirming that modulating the alkyl chain of the probe is an efficient strategy for optimizing the detection sensitivity to perchlorate by adjusting the van der Waals interaction.

Furthermore, based on the fluorescence decay curves (Figure S22), the C8-ClO_4 aggregates showed a much longer average fluorescence lifetime than the C8 probe, suggesting that the perchlorate anion in the aggregate might offer the non-covalent interactions, such as hydrogen bonds, to restrict the free rotation of the probe.[27] Therefore, the single-crystal parsing of the C8-ClO_4 aggregates was conducted to further identify and analyze the weak interactions between the C8 probe and perchlorate in detail. The solid-state structure of [C8]$(ClO_4)_2$ revealed the presence of C─H···O hydrogen bonds between the C8 probe and the perchlorate (Figure 2E). The highly polarized C─H bonds of pyridinium and the phenyl substituents engaged in dipole–anion interactions with the O of perchlorate as $d_{C-H\cdots O}$ = 2.481(9)–2.555(7) Å and $d_{C-H\cdots O}$ = 2.653(11)–3.091(10) Å, respectively (Figure 2F). Therefore, [C8]$(ClO_4)_2$ aggregates can emit strong fluorescence and are stable owing to the restricted rotation of the hydrogen bond.

To verify the interaction between the C8 probe and perchlorate in the crystal, Hirshfeld surface analysis was used to qualitatively analyze the non-covalent interaction force in a specific area of the probe.[28] From the results of the distance and curvature functions reflected in the Hirshfeld surface of C8 probe, it could be concluded that the interaction between the C8 probe and perchlorate anion was obviously dominant among over all interactions. The compact and concentrated red areas on the Hirshfeld surface of the C8 probe and perchlorate indicates the existence of strong non-covalent interactions, which could be attributed to the hydrogen bond interaction between the O atom in perchlorate and the H atom in the C8 probe (Figure 2Fi). From the 2D fingerprint plots for the local contact surface contribution of the C8 probe (Figure 2Fii), obtained by combining the distance from the internal and external nearest atom to the Hirshfeld surfaces (defined as d_i and d_e, respectively), the H atom in the C8 probe and the O atom in perchlorate have the closest distance (d = 2.35 Å), which reconfirmed the relatively stronger non-covalent interaction between the C8 probe and perchlorate. Moreover, in addition to the strength advantage, this non-covalent interaction (O─H) also occupied the largest area with 15.1% of the total Hirshfeld surface despite of the widespread weak H─H interaction between probe molecules caused by aggregation (Figure 2Fiii). Thus, both the van der Waals interaction and the hydrogen bond interaction between perchlorate and the C8 probe facilitates the aggregation process to restrict molecular rotation and results in green fluorescence emission.

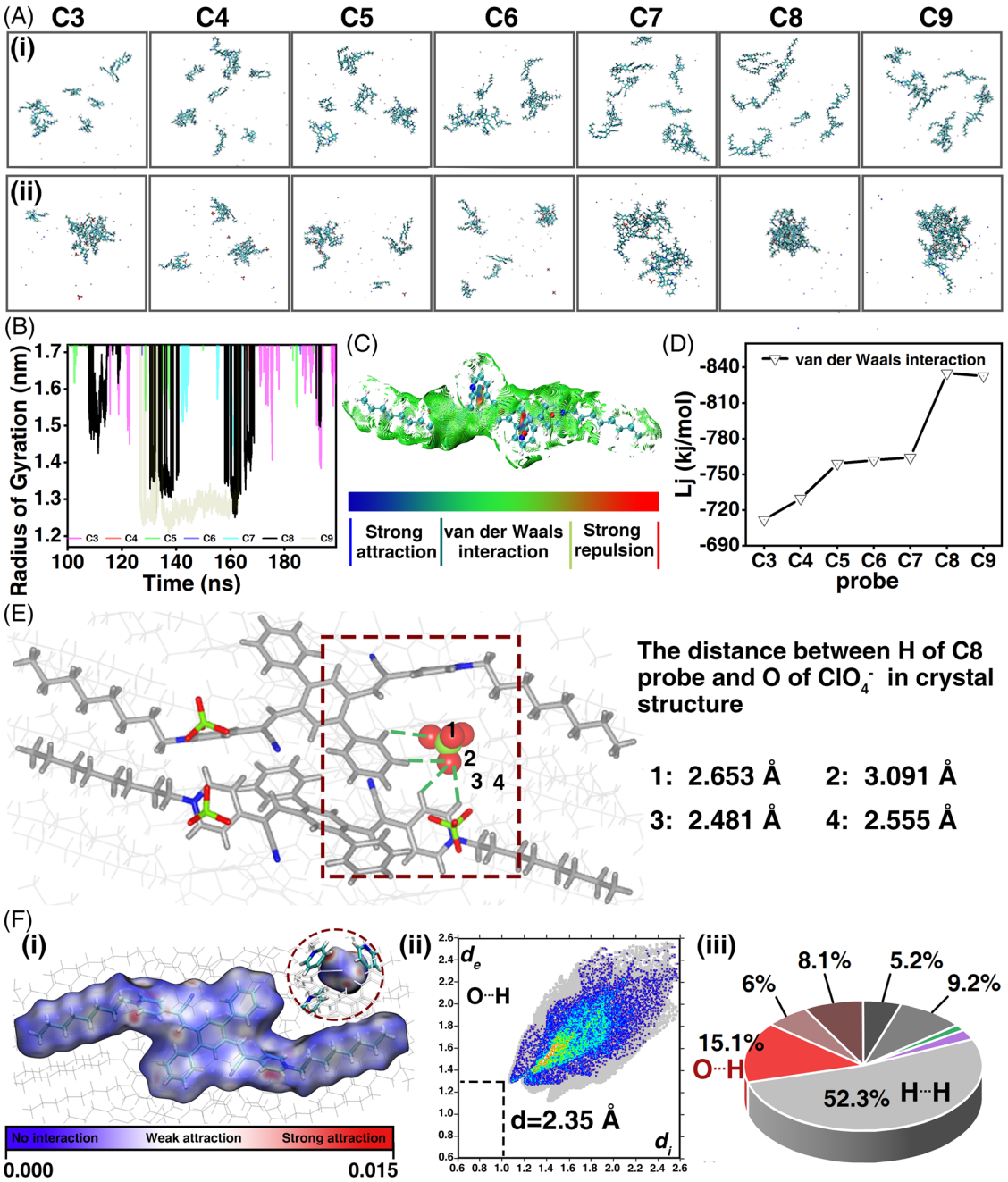

FIGURE 2 (A) Snapshot of molecular dynamics simulation of C3–C9 probe (i) alone and (ii) in the presence of perchlorate at 200 ns. (B) Radius of gyration of C3–C9 with perchlorate during 100–200 ns extracted from dynamic simulations. (C) Average non-covalent interaction between C8 probe and perchlorate. (D) The van der Waals interaction energies of C3–C9 with perchlorate calculated by molecular dynamics. (E) C—H···ClO_4^- hydrogen bonding (green dashed lines) in the crystal packing of C8-ClO_4 based on crystallographically determined atomic coordinates. (F) (i) The 3D Hirshfeld surfaces of the C8 probe surrounding perchlorates mapped by electron density under promolecular approximation cartography with color scheme varies in blue, white, and red, representing no interaction, weak attraction, and strong attraction, respectively, and (ii) the 2D fingerprint plots for the local contact surface contributed by O—H hydrogen bonds with the discrete gray clouds as the total Hirshfeld surface; and (iii) the contact surface area contributions of various fragments to the total Hirshfeld surface in the C8 probe

2.3 | Fluorescent sensing performance of C8 probe to perchlorate

The sensing performance of the C8 probe for perchlorate anions via the anion-induced AIE effect was evaluated. The fluorescent optical images of the C8 probe solution toward ClO_4^- with different concentrations showed an apparent change from no emission to bright green with the corresponding fluorescent intensity gradually increased with the concentration increasing from 0 to 10 mM (Figure 3A). Particularly, the probe solution with perchlorate of 0.5 mM showing green fluorescent emission with 365 nm UV illumination could be clearly distinguished from the blank probe solution by naked eye. Dynamic light scattering (DLS) results revealed that the diameter of the hydrodynamic aggregates increased from 10 nm to 2 μm with the addition of 5 equiv of perchlorate, indicating that the fluorescence turn-on process was accompanied by the formation of aggregates in the solution (Figure 3B). The fluorescence spectra showed that the characteristic emission peak at 530 nm for green fluorescence increased with increasing perchlorate concentration at 398 nm excitation (Figure 3C). Notably, the

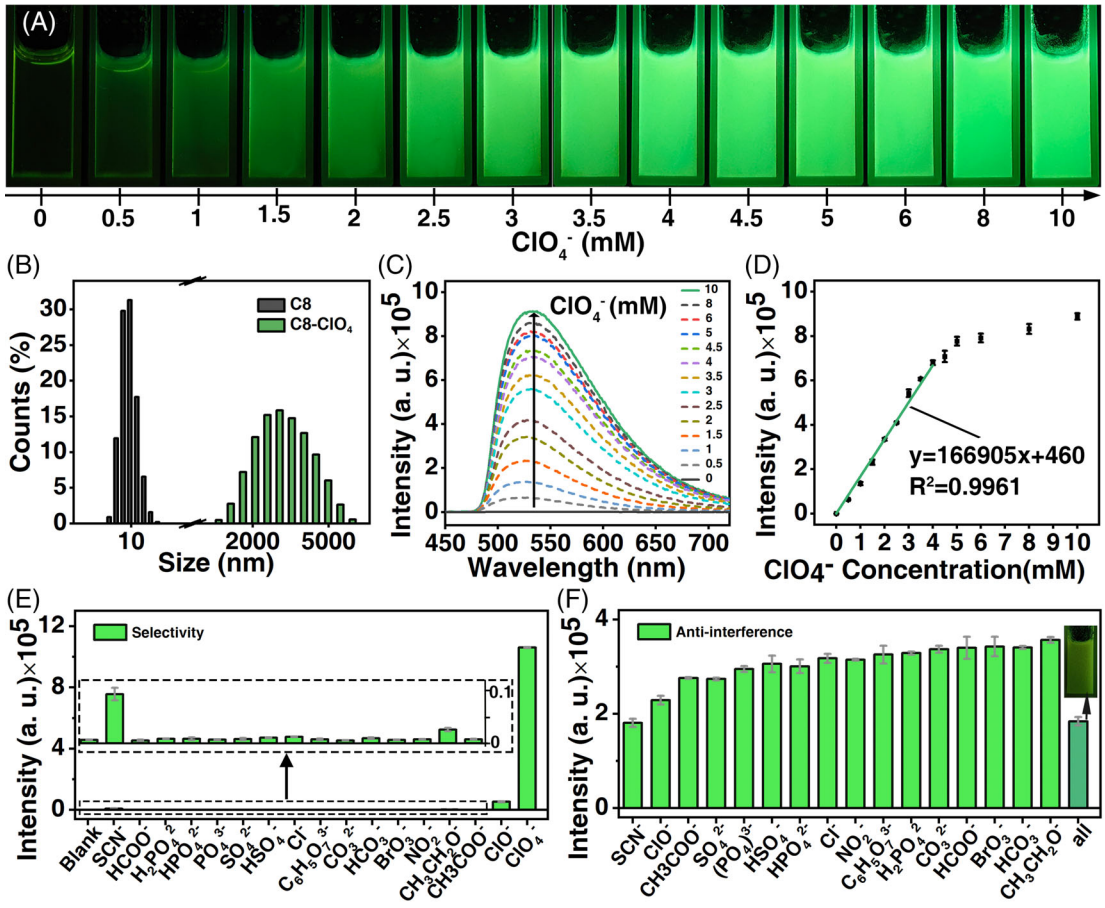

FIGURE 3 Fluorescent sensing performance of the C8 probe (2 mM) in glycol/0.1 M aqueous citric acid (3:2, v/v) mixed solution. (A) Images of C8 probe in response to perchlorate (0–10 mM) under 365 nm UV light. (B) Dynamic light scattering analysis of C8 probe with and without 10 mM perchlorate. (C) Fluorescence emission spectra of C8 probe upon addition of perchlorate (0–10 mM). (D) The relationship between the concentrations of ClO_4^- and the corresponding fluorescence intensities at 530 nm of C8 probe upon addition of perchlorate. (E) Selectivity of the C8 probe solution toward 5 equiv of perchlorate anion to other common anions with inset of the enlargement of the response toward the common anions. (F) Anti-interference ability of the C8 probe solution toward 5 equiv of perchlorate anion in the presence of other common anions separately or mixed together. The standard deviations were obtained from three repeated measurements

fluorescence intensities at 530 nm rise in a linear manner with respect to the increase of perchlorate concentration in the range of 0.5–5 mM (Figure 3D). According to the linear fitting slope (k = 167,233) of the fluorescence intensity, the limit of detection (LOD, defined as $3\sigma\ k^{-1}$, σ = 3) toward perchlorate was determined to be as low as 53.81 nM (~7 μg L^{-1}), which is much lower than the maximum limit of perchlorate (56 μg L^{-1}) stipulated by the Environmental Protection Agency[29] and proved to be premier compared with recently reported perchlorate probes (Table S2). The time-dependent observation of the response process of the 2 mM C8 probe to 25 equiv ClO_4^- showed that the probe responded immediately after the addition of perchlorate, and the response time could be defined as 5 s (video S2), indicating the rapid response of the probe.

Furthermore, the C8 probe solution showed a remarkable fluorescence turn-on response toward perchlorate with significant intensity enhancement from 0 to 10^5, while the 16 other common anions (Cl^-, NO_2^-, ClO^-, BrO_3^-, HCO_3^-, HSO_4^-, $H_2PO_4^-$, HPO_4^-, $HCOO^-$, Ac^-, $C_2H_5O^-$, SCN^-, CO_3^{2-}, SO_4^{2-}, PO_4^{3-}, $C_6H_5O_7^{3-}$) only lead to little fluorescent intensity increase (Figure 3E and its inset), indicating the good selectivity of the C8 probe toward the perchlorate anion. Besides, the anti-interference capability of the C8 probe was further evaluated by monitoring its sensing performance in the presence of perchlorate anion with the 16 other common anions co-existing respectively and all together. It could be concluded that most of the interfering anions alone had no apparent influence on the final characteristic fluorescence response toward perchlorate, with the emission intensity maintained at >70%, except for SCN^- (Figure 3F and Figure S23). The SCN^- revealed a fluorescence quenching effect of up to 45% of the original intensity for perchlorate, which could be attributed to the consumption of the highly oxidizing perchlorate anion by its reaction with the relatively reductive SCN^- anions.[30] More importantly, even with all the 16 interfering anions mixed up, the C8 probe still shows green fluorescence emission in the presence of ClO_4^-, indicating its excellent anti-interference capability (Figures 3F inset). The above results clearly demonstrate that C8 probe is highly selective, specific, and sensitive toward perchlorate, with an aggregation-induced turn-on feature facilitated by van der Waals interactions.

2.4 | Ultrasensitive detection of perchlorate particles

To further investigate the fluorescence-on sensing performance of the C8 probe toward perchlorate particles, the PAM

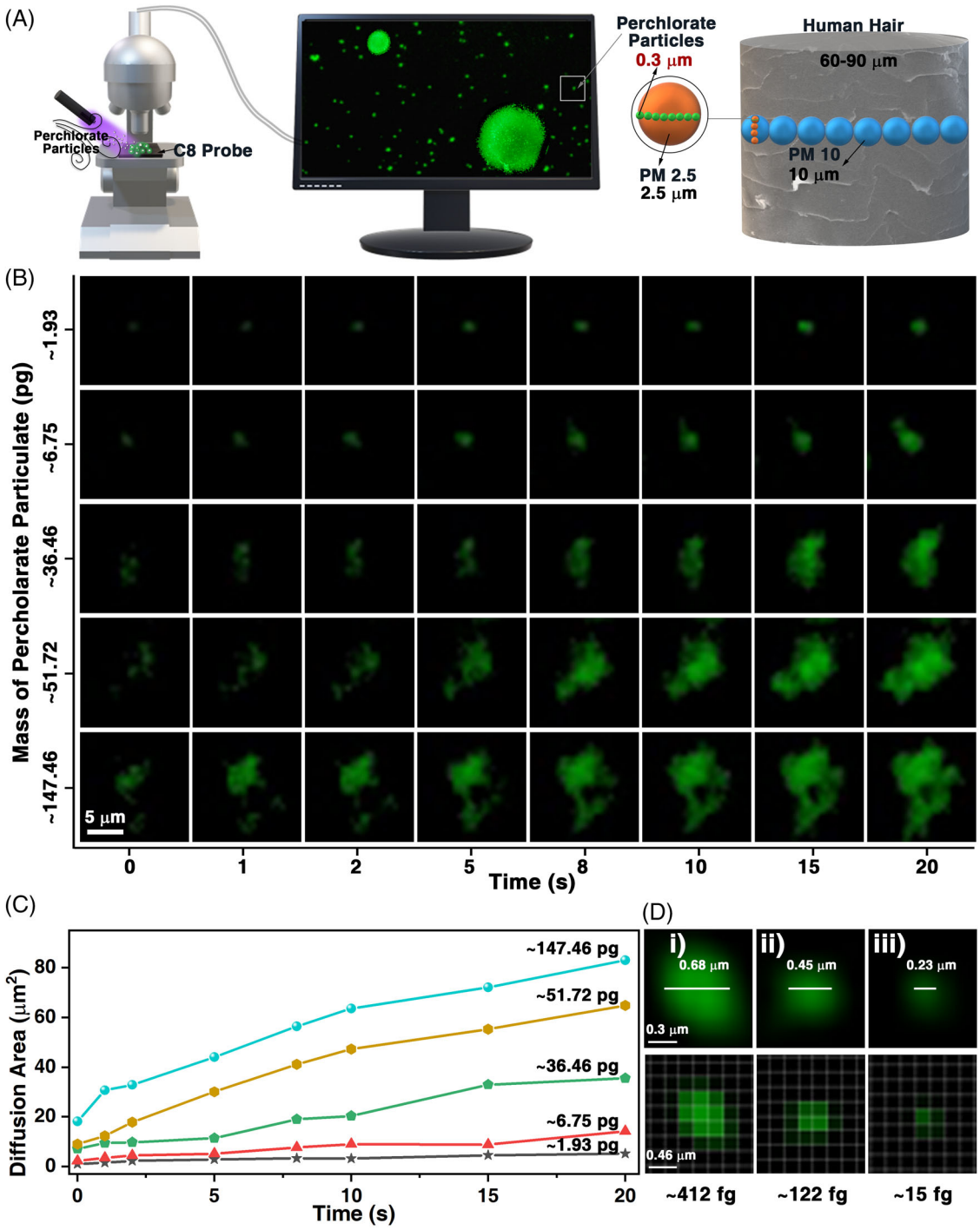

FIGURE 4 (A) Schematic diagram of the direct sensing of perchlorate particles by C8-PAM hydrogel with the diameter comparison of the detected perchlorate particle referring to human hair, PM 10 and PM 2.5. (B) Time-lapse images extracted from the video of the sensing process captured under a fluorescence microscope and (C) its corresponding diffusion area as a function of time. (D) The identification of the smallest perchlorate particles under fluorescence microscope observation

hydrogel loaded with the C8 probe was exposed to a great deal of perchlorate particles (Figure 4A). It is clear that upon contact with perchlorate particles, the C8 probe incorporated PAM hydrogel immediately show green fluorescence emission regardless of the particle size, which could be with a diameter of tens of microns as an individual human hair, in the range of 2.5–10 μm as the dust particles in polluted air, or even below 1 μm. The time-lapse fluorescent images of the green emitting patterns formed on the C8-PAM hydrogel in contact with perchlorate particles, which were extracted from the dynamic video of the detection of perchlorate particles with different masses, shows that all the fluorescence areas tended to increase with time owing to the dissolution and diffusion of the perchlorate particles (Figure 4B). Notably, the mass of an individual perchlorate particle was estimated based on the approximate circular size of the initial green emission, and the corresponding time was defined as 0 s. The fluorescence areas are larger and brighter for larger perchlorate particles, along with the more pronounced diffusion over time compared with small particles. According to the relationship between the diffusion area counted by pixels and time, it can be found that the large perchlorate particle with a mass of ~147.46 pg diffused from the initial area of 18 to 83 μm^2 within 20 s, while the diffusion of the small

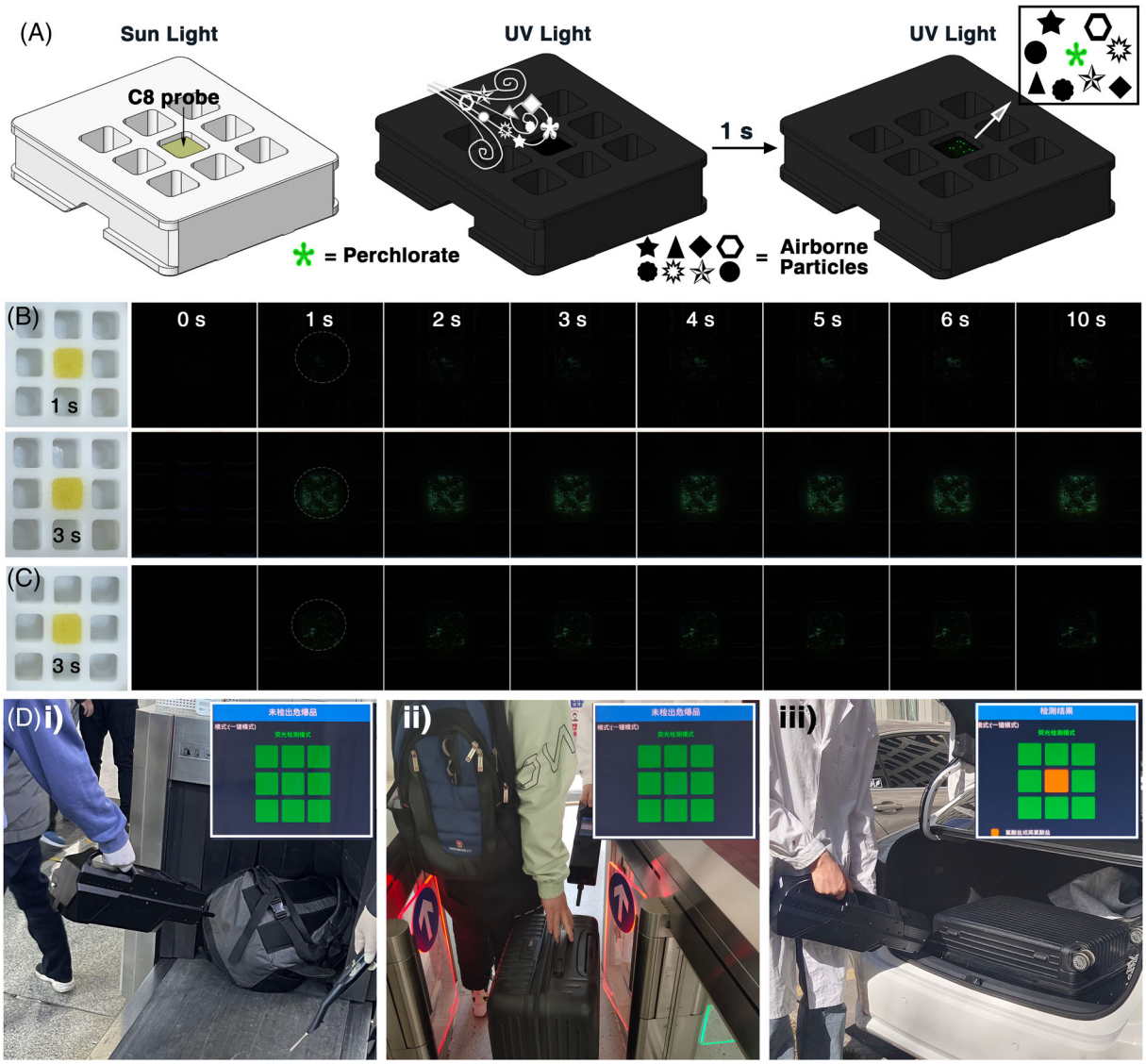

FIGURE 5 (A) Schematic diagram of the sensing chip for airborne perchlorate particulates detection. The real-time response image of the sensing chip incorporated in a portable explosive detector invented by our group after automatic pumping sample collection of the air (B) with only perchlorate particles for 1 and 3 s, and (C) with perchlorate, soil, sodium nitrite, sodium carbonate, sodium sulfate, potassium bisulfate, and calcium hypochlorite mixtures for 3 s. (D) Mock tests for the in-field detection of ultratrace perchlorate at security checking spots employing the detector on perchlorate-free bag and luggage (i) passing through an X-ray security inspection machine and (ii) at the entrance, and (iii) luggage with trace perchlorate residue in a car trunk with the test results shown in the insets

perchlorate particle with a mass of ~1.93 pg expanded from 1.01 to 5.22 μm^2 (Figure 4C). Although the diffusion ratios are almost the same, it should be noted that the brightness of the fluorescence signal was enhanced rather than weakened with the increase of perchlorate particle mass, implying that it is reasonable and conservative to estimate the mass of ultra-small particles through the final-state fluorescence area after diffusion. The detection limit is highly dependent on the spatial resolution of the fluorescence microscope employed, which is 0.23 μm per pixel in this case. The diffused fluorescence final area covering 3 × 3 pixels manifests that the mass of the corresponding perchlorate particle should not exceed 412 fg (Figure 4Di). For a particle with the corresponding fluorescence emission restrained in 2 × 2 pixels, the corresponding mass decreased to 122 fg (Figure 4Dii). Even when a particle was small enough to limit the resulting fluorescence area to only one pixel, the corresponding fluorescence emission could still be clearly observed and distinguished, indicating that the mass could be as low as 15 fg (Figure 4Diii). Therefore, the C8-PAM hydrogel sensing platform with high sensitivity and ultra-fast response is promising for ultratrace perchlorate particle detection.

2.5 | Practical applicability evaluation of the C8 probe to perchlorate particles

To further investigate the practical application of the C8 probe, a sensing chip was constructed from a porous polymer foam (Figure 5A). It is expected that the as-prepared sensing chip, which is yellow under sunlight and black under 365 nm UV light, would emit green fluorescence immediately when encountering perchlorate and would not be disturbed by other airborne particles. The sensing chip was incorporated into a portable explosive detector explored in our laboratory. By employing this detector and pumping air with perchlorate particles suspended for 1 s, green fluorescence emission spots appeared immediately on the sensing chip within 1 s

(Figure 5B). In addition, with the observation time extending to 10 s, the green emission spots tended to become increasingly larger and brighter. If the pumping time was extended to 3 s, the lightened spots would even cover the entire sensing chip with an observation time of only 1 s, and more remarkable green emission could be observed in the next 9 s, indicating the importance of pumping procedure for collecting perchlorate particles onto the surface of the sensing chip. Therefore, the air-pumping time was set to 3 s to ensure effective sample collection in practical scenarios. To further evaluate the reliability of the detector in sensing perchlorate particles in complex environments, air suspending samples were prepared with 10% mass ratio of perchlorate in mixing with soil and other interferents. The sensing chip can still immediately emit green fluorescence (Figure 5C), indicating good anti-interfering and highly reliable performance of the C8 probe for the rapid discrimination of perchlorate. Furthermore, this detector was applied in simulated tests for perchlorate-free and perchlorate-particle-polluted bags and luggage under various circumstances (Figure 5D). The detector could cooperate with the X-ray security inspection machine to finely screen possible residues or adsorbates on the bag surface. In addition, it could also be applied for rapid on-site checking of suspicious luggage carried by human beings or vehicles with alarm information involving the exact name of the suspected hazardous explosive substance, which is perchlorate in this case, once it is detected.

3 | CONCLUSION

In summary, it has been demonstrated that precise modulation of the alkyl chain length is of great influence for regulating the sensing performances of the oligo(p-phenylenevinylene) derivative AIE probe and achieving an excellent recognition capability toward the target analyte. The modulation of van der Waals interactions by the alkyl chain length enables efficient light-up detection of perchlorate with a low detection limit (53.81 nM), rapid response (<5 s), and excellent specificity even in the presence of 16 interfering anions mixture. The constructed hydrogel sensing device could achieve ultrasensitive detection of perchlorate particles as low as 15 fg under a fluorescence microscope. The proposed probe design strategy has proven to be reliable for exploring a portable detection platform, which significantly facilitate on-site detection of trace perchlorate in security checks. The present strategy is a promising candidate for detecting trace hazardous substances and AIE-based functional material conceptualization.

4 | EXPERIMENTAL SECTION

4.1 | Experimental details

Materials, general characterization, synthesis process of probes, single-crystal preparation and X-ray crystallography, sensing performance evaluation of C3–C9 probes to perchlorate, preparation and sensing testing of perchlorate solution and other analytes by C8 probe, preparation of C8-PAM hydrogel and sensing performance evaluation for perchlorate particles, preparation of the C8 porous polymer foam sensing chip and the detection of airborne particulates, are all placed in the Supporting Information.

4.2 | Calculation methods

The theoretical calculation in this work were conducted through the Gaussian software.[31] Subsequently, the wave function results were performed by the Multiwfn dev3.8.[32] The GROMACS package was used for the molecular dynamics simulation.[33] The VMD program[34] was used in the graphing of the molecular constructure. More details of the calculations are placed in the Supporting Information.

ACKNOWLEDGMENTS

This work was supported by the Natural Science Foundation of Xinjiang (2022D01E03), West Light Foundation of the Chinese Academy of Sciences (2021-XBQNXZ-023), National Natural Science Foundation of China (52172168, 22104152), Key Research Program of Frontier Sciences (CAS Grant No. ZDBS-LY-JSC029).

CONFLICT OF INTEREST

The authors declare no conflict of interest.

DATA AVAILABILITY STATEMENT

The data that support the findings of this study are available from the corresponding author upon reasonable request.

ORCID

Xincun Dou https://orcid.org/0000-0001-5825-9937

REFERENCES

1. a) R. E. Cook, P. J. Robinson, *Nature* **1982**, *299*, 674; b) R. B. Mellor, J. Ronnenberg, W. H. Campbell, S. Diekmann, *Nature* **1992**, *355*, 717.
2. a) P. A. Gale, C. Caltagirone, *Coord. Chem. Rev.* **2018**, *354*, 2; b) A. Docker, X. B. Shang, D. H. Yuan, H. K. Kuhn, Z. Y. Zhang, J. J. Davis, P. D. Beer, M. J. Langton, *Angew. Chem. Int. Ed.* **2021**, *60*, 19442.
3. a) G. F. Wang, Y. S. Li, Z. Z. Cai, X. C. Dou, *Adv. Mater.* **2020**, *32*, 1907043; b) X. Y. Hu, Z. W. Ma, J. G. Li, Z. Z. Cai, Y. S. Li, B. Y. Zu, X. C. Dou, *Mater. Horiz.* **2020**, *7*, 3250; c) G. Sriram, M. P. Bhat, P. Patil, U. T. Uthappa, H.-Y. Jung, T. Altalhi, T. Kumeria, T. M. Aminabhavi, R. K. Pai, Madhuprasad, M. D. Kurkuri, *TrAC, Trends Anal. Chem.* **2017**, *93*, 212.
4. J. J. Wang, Q. S. Chen, T. Belwal, X. Y. Lin, Z. S. Luo, *Compr. Rev. Food Sci. Food Saf.* **2021**, *20*, 2476.
5. S. Y. Wu, R. J. Xiao, H. Li, L. Q. Chen, *J. Mater. Chem. A* **2022**, *10*, 3093.
6. a) R. Hein, P. D. Beer, J. J. Davis, *Chem. Rev.* **2020**, *120*, 1888; b) L. J. Guo, Z. Yang, X. C. Dou, *Adv. Mater.* **2017**, *29*, 1; c) D. Fong, T. M. Swager, *J. Am. Chem. Soc.* **2021**, *143*, 4397.
7. a) X. C. Li, X. Liang, J. L. Yin, W. Y. Lin, *Chem. Soc. Rev.* **2021**, *50*, 102; b) Y. H. Tang, Y. Y. Ma, J. L. Yin, W. Y. Lin, *Chem. Soc. Rev.* **2019**, *48*, 4036; c) Y. F. Huang, Y. B. Zhang, F. J. Huo, Y. Wen, C. X. Yin, *Sci. China: Chem.* **2020**, *63*, 1742; d) P. Wang, F. Zhou, C. Zhang, S. Y. Yin, L. Teng, L. Chen, X. X. Hu, H. W. Liu, X. Yin, X. B. Zhang, *Chem. Sci.* **2018**, *9*, 8402; e) D. Barman, K. Narang, R. Parui, N. Zehra, M. N. Khatun, L. R. Adil, P. K. Iyer, *Aggregate* **2022**, *3*, e172.
8. a) N. Duan, H. Wang, Y. A. Li, S. X. Yang, H. Y. Tian, B. G. Sun, *Coord. Chem. Rev.* **2021**, *427*, 213557; b) A. Tarai, Y. Li, B. Liu, D. Zhang, J. Li, W. Yan, J. F. Zhang, J. L. Qu, Z. G. Yang, *Coord. Chem. Rev.* **2021**, *445*, 214070; c) S. H. Park, N. Kwon, J. H. Lee, J. Yoon, I. Shin, *Chem. Soc. Rev.* **2020**, *49*, 143; d) Z. W. Ma, J. G. Li, X. Y. Hu, Z. Z. Cai, X. C. Dou, *Adv. Sci.* **2020**, *7*, 2002991; e) P. X. Wang, Z. Z. Cai, J. G. Li, Y. S. Li, B. Y. Zu, X. C. Dou, *Adv. Optical Mater.* **2020**, *8*, 2000524; f) L. J. Xu, X. P. Jiang, K. Liang, M. Gao, B. Kong, *Aggregate* **2021**, *3*, e121; g) H. D. Li, H. Kim, J. J. Han, V. N. Nguyen, X. J. Peng, J. Y. Yoon, *Aggregate* **2021**, *2*, e51.

9. a) J. Y. Lee, H. D. Root, R. Ali, W. An, V. M. Lynch, S. Bahring, I. S. Kim, J. L. Sessler, J. S. Park, *J. Am. Chem. Soc.* **2020**, *142*, 19579; b) G. George, C. S. Edwards, J. I. Hayes, L. Yu, S. R. Ede, J. Wen, Z. Luo, *J. Mater. Chem. C* **2019**, *7*, 14949; c) X. C. Sun, Y. Wang, Y. Lei, *Chem. Soc. Rev.* **2015**, *44*, 8019; d) H. Zhou, M. H. Chua, B. Z. Tang, J. W. Xu, *Polym. Chem.* **2019**, *10*, 3822; e) T. S. Zhang, X. Y. Hu, B. Y. Zu, X. C. Dou, *Adv. photonics* **2022**, *3*, 2200006; f) C. Q. Cheng, Y. J. Gong, Y. X. Guo, L. F. Cui, H. W. Ji, H. Yuan, L. Jiang, J. C. Zhao, Y. K. Che, *Angew. Chem. Int. Ed.* **2021**, *60*, 5827.
10. a) N. Garg, A. Deep, A. L. Sharma, *Coord. Chem. Rev.* **2021**, *445*, 214073; b) P. Zheng, A. Abdurahman, Z. X. Zhang, Y. T. Feng, Y. M. Zhang, X. Ai, F. Li, M. Zhang, *J. Hazard. Mater.* **2021**, *409*, 124500; c) X. M. Chang, Z. X. Zhou, C. D. Shang, G. Wang, Z. L. Wang, Y. Y. Qi, Z. Y. Li, H. Wang, L. P. Cao, X. P. Li, Y. Fang, P. J. Stang, *J. Am. Chem. Soc.* **2019**, *141*, 1757; d) Y. T. Lei, G. H. Zhang, Q. L. Zhang, L. Yu, H. Li, H. L. Yu, Y. He, *Nat. Commun.* **2021**, *12*, 4483; e) R. R. Huang, M. Q. Li, D. H. Lin, Y. T. Shao, C. D. Shang, Q. Q. Liu, G. J. Liu, N. Li, R. Miao, H. N. Peng, Y. L. Tang, Y. Fang, *Aggregate* **2022**, *3*, e203.
11. a) S. D. Xu, Y. K. Duan, B. Liu, *Adv. Mater.* **2020**, *32*, 1903530; b) J. Li, J. X. Wang, H. X. Li, N. Song, D. Wang, B. Z. Tang, *Chem. Soc. Rev.* **2020**, *49*, 1144; c) N. Meher, P. K. Iyer, *Angew. Chem. Int. Ed.* **2018**, *57*, 8488; d) J. G. Wang, X. G. Gu, P. F. Zhang, X. B. Huang, X. Y. Zheng, M. Chen, H. T. Feng, R. T. K. Kwok, J. W. Y. Lam, B. Z. Tang, *J. Am. Chem. Soc.* **2017**, *139*, 16974.
12. a) J. Mei, N. L. C. Leung, R. T. K. Kwok, J. W. Y. Lam, B. Z. Tang, *Chem. Rev.* **2015**, *115*, 11718; b) P. Alam, N. L. C. Leung, J. Zhang, R. T. K. Kwok, J. W. Y. Lam, B. Z. Tang, *Coord. Chem. Rev.* **2021**, *429*, 213693; c) J. Zhang, B. Z. He, Y. B. Hu, P. Alam, H. K. Zhang, J. W. Y. Lam, B. Z. Tang, *Adv. Mater.* **2021**, *33*, 2008071; d) M. H. Chua, K. W. Shah, H. Zhou, J. W. Xu, *Molecules* **2019**, *24*, 2711; e) X. L. Huang, Q. Guo, R. Y. Zhang, Y. K. Leng, J. W. Y. Lam, Y. H. Xiong, T. B. Zhong, *Compr. Rev. Food Sci. Food Saf.* **2020**, *19*, 2297; f) C. Chen, H. Q. Gao, H. L. Ou, R. T. K. Kwok, Y. H. Tang, D. H. Zheng, D. Ding, *J. Am. Chem. Soc.* **2022**, *144*, 3429; g) Y. Z. Liu, X. Y. Guan, Q. R. Fang, *Aggregate* **2021**, *2*, e34; h) R. Hu, A. J. Qin, B. Z. Tang, *Prog. Polym. Sci.* **2020**, *100*, 101176.
13. a) D. Oelkrug, A. Tompert, J. Gierschner, E. Hans-Joachim, M. Hanack, M. Hohloch, E. Steinhuber, *J. Phys. Chem. B* **1998**, *102*, 1902; b) F. Wurthner, *Angew. Chem. Int. Ed.* **2020**, *59*, 14192; c) S. Suzuki, S. Sasaki, A. S. Sairi, R. Iwai, B. Z. Tang, G. I. Konishi, *Angew. Chem. Int. Ed.* **2020**, *59*, 9856.
14. a) W. G. Qiao, T. Ma, S. S. Wang, L. J. Li, M. Liu, H. Jiang, Y. Z. Wu, J. T. Zhu, Z. A. Li, *Adv. Funct. Mater.* **2021**, *31*, 2105452; b) H. Feng, J. P. Liu, A. Qaitoon, Q. T. Meng, Y. Sultanbawa, Z. Q. Zhang, Z. P. Xu, R. Zhang, *TrAC Trends Anal. Chem.* **2021**, *136*, 116199; c) H. B. Wan, Q. F. Xu, P. Y. Gu, H. Li, D. Y. Chen, N. J. Li, J. H. He, J. M. Lu, *J. Hazard. Mater.* **2021**, *403*, 123656; d) D. Cheng, J. J. Peng, Y. Lv, D. D. Su, D. J. Liu, M. Chen, L. Yuan, X. B. Zhang, *J. Am. Chem. Soc.* **2019**, *141*, 6352.
15. a) A. Sahana, A. Banerjee, S. Lohar, A. Chottapadhyay, S. K. Mukhopadhyay, D. Das, *RSC Adv*. **2013**, *3*, 14044; b) R. Kumar, S. Sandhu, P. Singh, S. Kumar, *J. Mater. Chem. C* **2016**, *4*, 7420; c) S. Y. Chen, X. L. Ni, *RSC Adv.* **2016**, *6*, 6997.
16. S. J. Liu, X. Zhou, H. K. Zhang, H. L. Ou, J. W. Y. Lam, Y. Liu, L. Q. Shi, D. Ding, B. Z. Tang, *J. Am. Chem. Soc.* **2019**, *141*, 5359.
17. a) N. Li, Y. Y. Liu, Y. Li, J. B. Zhuang, R. R. Cui, Q. Gong, N. Zhao, B. Z. Tang, *ACS Appl. Mater. Interfaces* **2018**, *10*, 24249; b) Y. Yang, S. Chen, X. L. Ni, *Anal. Chem.* **2015**, *87*, 7461.
18. J. D. Coates, L. A. Achenbach, *Nat. Rev. Microbiol.* **2004**, *2*, 569.
19. a) C. X. Ren, P. Yang, J. N. Sun, E. Y. Bi, J. Y. Gao, J. Palmer, M. Q. Zhu, Y. Y. Wu, J. Y. Liu, *J. Am. Chem. Soc.* **2021**, *143*, 7891; b) K. W. Loach, *Nature* **1962**, *24*, 754; c) Z. Su, Y. S. Li, J. G. Li, X. C. Dou, *Sens. Actuators, B* **2021**, *336*, 129728; d) S. E. Beacom, *Nature* **1959**, *183*, 38; e) Z. Su, Y. S. Li, J. G. Li, K. Li, X. C. Dou, *J. Mater. Chem. A* **2022**, *10*, 8195.
20. J. Watson, 2018 Explosives Incident Report, United States Bomb Data Center (USBDC), Huntsville **2018**.
21. a) C. L. Ford, Y. J. Park, M. M. Ellen, G. Zachary, R. F. Alison, *Science* **2016**, *354*, 741; b) M. R. Walsh, M. E. Walsh, C. A. Ramsey, S. Brochu, S. Thiboutot, G. Ampleman, *J. Hazard. Mater.* **2013**, *262*, 228; c) D. Karunanidhi, P. Aravinthasamy, T. Subramani, H. A. H. C. Jayasena, *Exposure Health* **2021**, *14*, 359.
22. E. F. S. Authority, *EFSA J.* **2014**, *12*, 3869.
23. a) V. Vinson, *Science* **2020**, *27*, 533; b) J. Wolff, *Pharmacol. Rev.* **1998**, *50*, 89.
24. U. V. D. Leyen, *Off. J. Eur. Communities* **2020**, *L160*, 3.
25. a) R. Kumar, S. Sandhu, P. Singh, S. Kumar, *J. Mater. Chem. C* **2016**, *4*, 7420; b) P. Singh, L. S. Mittal, V. Vanita, R. Kumar, G. Bhargava, A. Walia, S. Kumar, *Chem. Commun.* **2014**, *50*, 13994; c) X. B. Zheng, R. Q. Fan, K. Xing, K. Zhu, P. Wang, Y. L. Yang, *Chem. Eng. J.* **2020**, *380*, 122580.
26. S. Kim, J. Kim, D. Lee, *Angew. Chem. Int. Ed.* **2021**, *60*, 10858.
27. Z. J. Luo, T. Y. Z. Lv, K. N. Zhu, Y. Li, L. Wang, J. J. Gooding, G. Z. Liu, B. Liu, *Angew. Chem. Int. Ed.* **2020**, *59*, 3131.
28. M. A. Spackman, D. Jayatilaka, *CrystEngComm* **2009**, *11*, 19.
29. a) K. M. Morley, *J. Am. Water Works Assoc.* **2020**, *112*, 8; b) A. Llorente-Esteban, R. W. Manville, A. Reyna-Neyra, G. W. Abbott, L. M. Amzel, N. Carrasco, *Nat. Struct. Mol. Biol.* **2020**, *27*, 533.
30. N. N. Greenwood, A. Earnshaw, *Chemistry of the elements*, Elsevier Butterworth-Heinemann, Burlington, MA, **1989**.
31. M. J. Frisch, G. W. Trucks, H. B. Schlegel, G. E. Scuseria, M. A. Robb, J. R. Cheeseman, G. Scalmani, V. Barone, G. A. Petersson, H. Nakatsuji, X. Li, M. Caricato, A. V. Marenich, J. Bloino, B. G. Janesko, R. Gomperts, B. Mennucci, H. P. Hratchian, J. V. Ortiz, A. F. Izmaylov, J. L. Sonnenberg, Williams, F. Ding, F. Lipparini, F. Egidi, J. Goings, B. Peng, A. Petrone, T. Henderson, D. Ranasinghe, V. G. Zakrzewski, J. Gao, N. Rega, G. Zheng, W. Liang, M. Hada, M. Ehara, K. Toyota, R. Fukuda, J. Hasegawa, M. Ishida, T. Nakajima, Y. Honda, O. Kitao, H. Nakai, T. Vreven, K. Throssell, J. A. Montgomery Jr., J. E. Peralta, F. Ogliaro, M. J. Bearpark, J. J. Heyd, E. N. Brothers, K. N. Kudin, V. N. Staroverov, T. A. Keith, R. Kobayashi, J. Normand, K. Raghavachari, A. P. Rendell, J. C. Burant, S. S. Iyengar, J. Tomasi, M. Cossi, J. M. Millam, M. Klene, C. Adamo, R. Cammi, J. W. Ochterski, R. L. Martin, K. Morokuma, O. Farkas, J. B. Foresman, D. J. Fox, Gaussian 16, Rev. C.01; Gaussian, Inc.: Wallingford, CT, **2016**.
32. T. Lu, F. Chen, *J. Comput. Chem.* **2012**, *33*, 580.
33. a) M. J. Abraham, T. Murtola, R. Schulz, S. Páll, J. C. Smith, B. Hess, E. Lindahl, *SoftwareX* **2015**, *1–2*, 19; b) S. Pronk, S. Páll, R. Schulz, P. Larsson, P. Bjelkmar, R. Apostolov, M. R. Shirts, J. C. Smith, P. M. Kasson, D. van der Spoel, B. Hess, E. Lindahl, *Bioinformatics* **2013**, *29*, 845.
34. W. Humphrey, A. Dalke, K. Schulten, *J. Mol. Graphics Modell.* **1996**, *14*, 33.

SUPPORTING INFORMATION

Additional supporting information can be found online in the Supporting Information section at the end of this article.

How to cite this article: F. Xiao, Y. Li, J. Li, D. Lei, G. Wang, T. Zhang, X. Hu, X. Dou, *Aggregate* **2022**, e260. https://doi.org/10.1002/agt2.260